communications physics

ARTICLE

https://doi.org/10.1038/s42005-023-01169-1 OPEN

Ultrafast hole relaxation dynamics in quantum dots revealed by two-dimensional electronic spectroscopy

Patrick J. Brosseau[1], Jaco J. Geuchies[2], Dipti Jasrasaria[3], Arjan J. Houtepen[2], Eran Rabani[3,4,5] & Patanjali Kambhampati[1✉]

Elucidating the population dynamics of correlated electron-hole pairs (bound excitons) in semiconducting quantum dots (QDs) is key for developing our fundamental understanding of nanoscale photophysics as well as for the optimal design of devices, such as lasers. For decades, it was assumed that holes did not contribute to band edge bleach signals in QDs. Here, we employ two-dimensional electronic spectroscopy to monitor electron and hole dynamics in both CdSe and CdSe/CdS/ZnS QDs to probe electron and hole dynamics. Based on a combination of time and frequency resolution, we observe a previously unresolved bleaching signal in CdSe QDs on timescales faster than 30 fs due to hole cooling. Atomistic semiempirical pseudopotential calculations are used to rationalize the order of magnitude difference in the observed hole dynamics in CdSe and CdSe/CdS/ZnS QDs. This picture advances our understanding of QD excitonics past the prevailing continuum effective mass theories generally used to describe QD electronic structure and dynamics.

[1] Department of Chemistry, McGill University, Montreal, Québec, Canada. [2] Optoelectronic Materials Section, Faculty of Applied Sciences, Delft University of Technology, Delft, The Netherlands. [3] Department of Chemistry, University of California, Berkeley, CA 94720, USA. [4] Materials Sciences Division, Lawrence Berkeley National Laboratory, Berkeley, CA 94720, USA. [5] The Sackler Center for Computational Molecular and Materials Science, Tel Aviv University, Tel Aviv 69978, Israel. ✉email: pat.kambhampati@mcgill.ca

Semiconductor quantum dots (QDs) have been widely studied since their discovery in the 1980s, and they have become a canonical material in the study of nanoscale photophysics[1–6]. Using a variety of techniques, ranging from single dot photoluminescence (PL)[7–9] to ultrafast spectroscopies, such as transient absorption (TA) spectroscopy[10–13], rich excitonic dynamics on diverse timescales have been observed. However, some mysteries remain to date. One of the main observations made is that holes do not appear to contribute to the bleaching signals in TA experiments that are now commonplace[10,14]. However, the measurement of amplified stimulated emission (ASE) in QDs implies that hole-bleaching signals must be present[11,15]. Recent TA experiments have revisited this problem and have proven inconclusive or contradictory[15–18]. Yet the ability to count charge carriers (i.e., electrons and holes) is of paramount importance to furthering our understanding of the electronic structure and dynamics of QDs, and it has direct consequences for the design of QD-based optoelectronic devices, such as photovoltaics[19], lasers[20], and light-emitting diodes[21].

In TA experiments, a decrease in sample absorbance can be due to ground-state bleach (GSB) and/or stimulated emission (SE), while an increase in absorbance is due to excited-state absorption (ESA), as detailed in Supplementary Note 1. The experimentally observed TA signal, ΔOD, measures these non-linear modifications (GSB, SE, ESA) to the sample's linear absorbance, OD_0. In many semiconducting QDs, such as CdSe and CdS, the heavier hole effective mass and high degeneracy of hole states would lead to a higher density of states in the valence band than in the conduction band. Thus, while the presence of a single exciton in a QD would lead to significant saturation of the electronic transition at room temperature, there would be minimal saturation of individual hole transitions, and hole dynamics would not be reflected in the bleach[10]. To test this hypothesis, a number of TA experiments have been performed on CdSe QDs. In initial state-resolved pump/probe (SRPP) experiments, a variation on TA spectroscopy in which states are selectively excited, no sign of hole bleach in core-only CdSe QDs was observed by resonantly pumping into the X_1 or X_2 transitions (see Fig. 1a, b) with 70 fs time resolution[22]. In recent SRPP experiments with 130 fs time resolution, hole contributions to the bleach were not resolved in non-surface-engineered CdSe QDs, but hole contributions to the bleach were measured in $InCl_3$ surface treated core-only CdSe QDs and core/shell CdSe/CdS/ZnS QDs[15]. Indeed, a time constant of 210 fs ± 20 fs was attributed to the X_2 to X_1 relaxation in CdSe/CdS/ZnS QDs[15]. The presence of a hole bleach was further confirmed by spectroelectrochemical hole injection measurements, and TA gain measurements[15].

Recent TA experiments with 10 fs time resolution did not find evidence for fast hole trapping leading to the hole bleach in core-only CdSe QDs[17]. However, other recent TA studies with hole-accepting ligands[16] and electron-accepting ligands[18] provide conflicting evidence for whether holes contribute to the TA bleach. Furthermore, the argument for why holes were not observed in 1D TA spectra[15,18,23], namely hole trapping on timescales of ~30 fs, seems inconsistent with other measurements of hole trapping[17,24,25]. In summary, the most recent data have not yet provided a conclusive picture regarding the contribution of holes to the bleaching signals of simple TA spectra of QDs.

These conflicting observations suggest that a more correlated approach, which can directly observe the hole dynamics, is needed. Most prior experiments are based on a one-dimensional ultrafast probe, which offers limited information on correlated transitions due to a lack of time resolution and energy resolution, information that is provided by two-dimensional electronic spectroscopy (2DES)[26]. Applying this approach to studying the photophysics of CdSe QDs allows one to selectively excite the X_2 transition and monitor the relaxation from X_2 to X_1 on ultrafast timescales[27–30]. Previous 2DES experiments on semiconductor QDs have measured either hole relaxation times[28–30] or band-edge excited-state absorption (ESA) dynamics[31,32], but a full analysis of hole contributions to both the bleach and ESA in both core-only and core/shell QDs is still lacking.

Here, we perform ultrafast 2DES on both model core-only CdSe QDs and surface-engineered CdSe/CdS/ZnS core/shell QDs. 2DES experiments on the core-only CdSe QDs confirm that there is no sign of hole trapping with either X_1 or X_2 excitation, but rather that the hole relaxes to the band edge on a previously unresolvable 30 fs timescale. The 2DES experiments confirm previous 1D TA experiments on the surface-engineered core/shell QDs[15,18,23], which show that holes do contribute to bleaching signals, and provide new observations about ESA due to biexcitons, to the best of our knowledge. Both the fast timescale of hole relaxation and the excitation photon energy dependence of ESA suggest the presence of a quasi-continuous valence band. Atomistic electronic structure calculations are used to rationalize these experimental findings and explain the order of magnitude

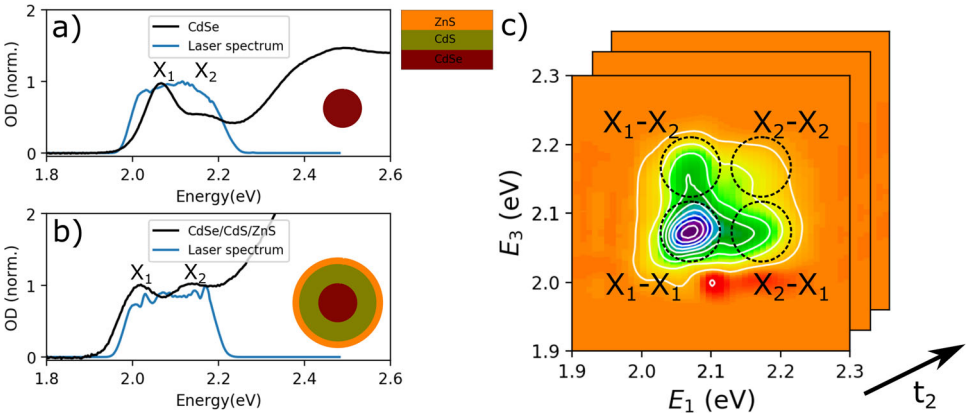

Fig. 1 Schematic overview of two-dimensional electronic spectroscopy (2DES) as a probe of the electronic structure of quantum dots. a Linear absorption spectrum of CdSe quantum dots (QDs) in black and laser spectrum used in 2DES experiment in blue, where OD is the normalized optical density. X_1 is the first excitonic state and X_2 is the second excitonic state. **b** Linear absorption spectrum of CdSe/CdS/ZnS core/shell QDs in black and laser spectrum used in 2DES experiment in blue. The insets in panels a and b show the QD material layers. **c** Diagram labeling the four main peaks in the 2DES spectrum for CdSe QDs. The peaks are labeled by the excitation state followed by the emission state. E_1 is the 2DES excitation energy, E_3 is emission energy, and t_2 is the time delay between the pump pulses and the probe pulse.

difference between the timescales of relaxation in the core-only and core/shell systems. The results conclusively identify ultrafast 30 fs hole cooling as the reason why the hole contribution to the absorption bleach in TA spectra has remained elusive so far and explain the order of magnitude difference in timescales of hole and electron cooling, as well as the much faster hole cooling in core-only CdSe QDs compared to core–shell QDs. These 2DES results reveal the need for atomistic theories to rigorously understand the electronic structure and dynamics of QDs.

Results and discussion

The X_1 and X_2 transitions of CdSe QDs provide a convenient testbed for measuring the relative contributions of electrons and holes to the excitonic transitions in spectroscopic data. The X_1 and X_2 transitions share an electron state but differ in their contribution of hole states, so differences in the spectroscopic signatures of these two states can generally be attributed to holes[15,22]. The X_1 and X_2 transitions appear as two distinct absorption features in the steady-state absorption spectrum of CdSe QD, as shown in Fig. 1a. The absorption spectrum of core/shell–shell CdSe/CdS/ZnS QD, shown in Fig. 1b, also features two distinct peaks, labeled X_1 and X_2. The pulse spectra used for 2DES experiment are also shown in blue in Fig. 1a, b. The 2DES spectra of CdSe in Fig. 1c show four bleaching features, labeled X_1–X_1, X_1–X_2, X_2–X_1, and X_2–X_2. The transition before the dash represents the excitation while the transition after the dash represents the emission. Therefore, the X_2–X_1 cross-peak corresponds to pumping into the X_2 transition then probing the X_1 transition. The population time, t_2, is analogous to the pump-probe time delay in TA. The intensity of the X_2–X_1 peak as a function of t_2 can be used to track the relaxation from X_2 to X_1, mainly attributed to hole relaxation, as detailed in Supplementary Note 2. Due to overlapping GSB, SE and ESA signals, an increase in the X_2–X_1 peak amplitude may reflect an increase in GSB or SE or a decrease in the overlapping ESA signal, as detailed in Supplementary Note 8.

Figure 2 depicts 2DES spectra at a range of population time delays, t_2, for both the CdSe/CdS/ZnS and CdSe QDs. At $t_2 = 20$ fs, the pump and probe pulses are still partially overlapping and the 2D lineshapes contain additional signals, as discussed below and in Supplementary Note 5. By $t_2 = 100$ fs the 2D peaks can be clearly resolved from the non-resonant signals. In CdSe/CdS/ZnS, the signal intensity of the X_2–X_1 peak in the lower right-hand corner of the 2DES spectrum increases from $t_2 = 100$ fs to 200 fs, indicating relaxation from X_2 to X_1. In CdSe, however, there is no significant change in the X_2-X_1 peak between $t_2 = 100$ fs and 200 fs, signifying that the X_2 to X_1 relaxation has already occurred by 100 fs. The CdSe 2DE spectra show positive ESA peaks at probe energies below $E_3 = 2.0$ eV that decay between $t_2 = 100$ fs and $t_2 = 200$ fs. The ESA in this region reflects a redshift of the X_1 peak in excited QDs while GSB reflects state filling of the X_1 state. The ESA can be disentangled from the GSB and SE as the ESA creates positive features in the 2DE spectra[24,33,34]. While the dynamics of both the GSB and ESA reflect the population of the single-exciton states, the ESA reflects spectral dynamics that are not evident within the GSB or SE, which will be shown in more detail in the following figures. These 2DE spectra reveal the richness in the data that is not captured by 1D TA spectroscopy, as is often found in 2D spectroscopy[30,35–37].

Transient exciton dynamics. While the 2DES contour maps are useful for showing energetic interactions, they are less useful for observing the dynamics. To directly monitor the carrier dynamics, we perform projections of the 2DES plots onto pseudo-TA spectra. By virtue of the 2DES method, one can have E_1 projections and E_3 projections, where E_1 projections refer to an excitation spectrum and E_3 projections refer to an emission (pseudo-TA) spectrum. The pseudo-TA spectra are obtained by spectral integration of a window in the conjugate energy axis, as shown in Supplementary Note 3. These energetic projections allow for high excitation energy resolution while maintaining high time resolution, which is not possible in 1D TA spectroscopy.

One-dimensional pseudo-TA spectra can be generated from 2DES spectra by integrating over a range of excitation energies, as shown in Supplementary Fig. S3. In the case of the CdSe pseudo-TA spectra in Fig. 3, three distinct features can be identified. From low energy to high energy, they are positive ESA from the single exciton to biexciton transition, negative bleaching from probing the X_1 transition, and negative bleaching from probing the X_2 transition. The position of the ESA peak relative to the X_1 bleach is determined by the biexciton binding energy[10]. The ESA is not as apparent in the CdSe/CdS/ZnS pseudo-TA spectra in Fig. 3a, b. The biexciton binding energy may be different in the CdSe/CdS/ZnS QD due to delocalization of the electronic wavefunction into the CdS shell[38], and may even be repulsive rather than attractive[39,40]. The transitions from excitons to biexcitons involve a rich spectrum, not a single transition from X to XX[31,33,41–44]. In CdSe/CdS/ZnS, an X_1 pump creates an IRF-limited bleach while the pseudo-TA spectrum with an X_2 pump gradually grows (Fig. 3). This pump dependence of the X_1 bleach in CdSe/CdS/ZnS TA spectra has been previously attributed to a hole bleach[15]. These 2DES results, with 30 fs time resolution, confirm the prior 1D TA measurements done with 130-fs time resolution[15,23].

By spectrally integrating the E_3 projections, the early time response of the QD can be monitored precisely with kinetic transients of the X_1–X_1 and X_2–X_1 peaks, as shown in the side panels in Fig. 3. The transients are generated by integrating within a radius centered on the X_1–X_1 and X_2–X_1 peaks, as is standard within the 2DES community[28,30] and as detailed in Supplementary Note 4. The kinetic transient of the X_2–X_1 cross-peak in the CdSe/CdS/ZnS QD shows a fast IRF-limited bleach followed by a slow decay. The time constant of the slow decay is $300 +/- 60$ fs, and the slow component accounts for 40% of the bleach, as detailed in Supplementary Note 7. The fast component is attributed to an instantaneous bleach from electronic states shared by the X_1 and X_2 transitions. The slow component is attributed to a hole bleach that grows in as the hole relaxes across the $X_2 \rightarrow X_1$ transition. Previous studies measured that the slow component attributed to hole cooling comprises 33% of the bleach[15,23]. It has been noted that the hole contribution to the bleach may vary between samples, which is attributed to differences in the fine structure splitting[18]. Adding a CdS shell to a CdSe QD fundamentally alters the excitonic structure, including the fine structure, as the electron wavefunction can delocalize into the CdS shell. The degree of delocalization depends on the shell thickness, so variation in CdS shell thicknesses between samples could account for differences in the measured ratio of electron and hole bleach.

For the case of CdSe QDs, the bleaching signal evolves nearly an order of magnitude more rapidly than in CdSe/CdS/ZnS. In CdSe, the X_2–X_1 cross-peak fully relaxes within the first 50 fs. The challenge with any ultrafast spectroscopy is the non-resonant signals arriving during pulse overlap or reversed order pulses. These early time delay signals have fortunately been well discussed in the literature[45–50] and are further discussed in Supplementary Note 5. From the data, we can extract an estimate of the timescale of the resonant dynamics. We estimate that the resonant contributions to the bleaching signal in CdSe take place on a ~30 fs timescale, nearly an order of magnitude faster than the CdSe/CdS/ZnS system. The X_1–X_1 transients in both the CdSe and CdSe/CdS/ZnS QDs also reveal coherent oscillations, due to coupling between the exciton and the LO phonon mode, as shown in Supplementary Note 9. When the coherent oscillations are normalized by the absolute amplitude of the 2DES signal, the intensity of the coupling to the LO phonon is 1.15 times stronger in CdSe. While the bleach dynamics

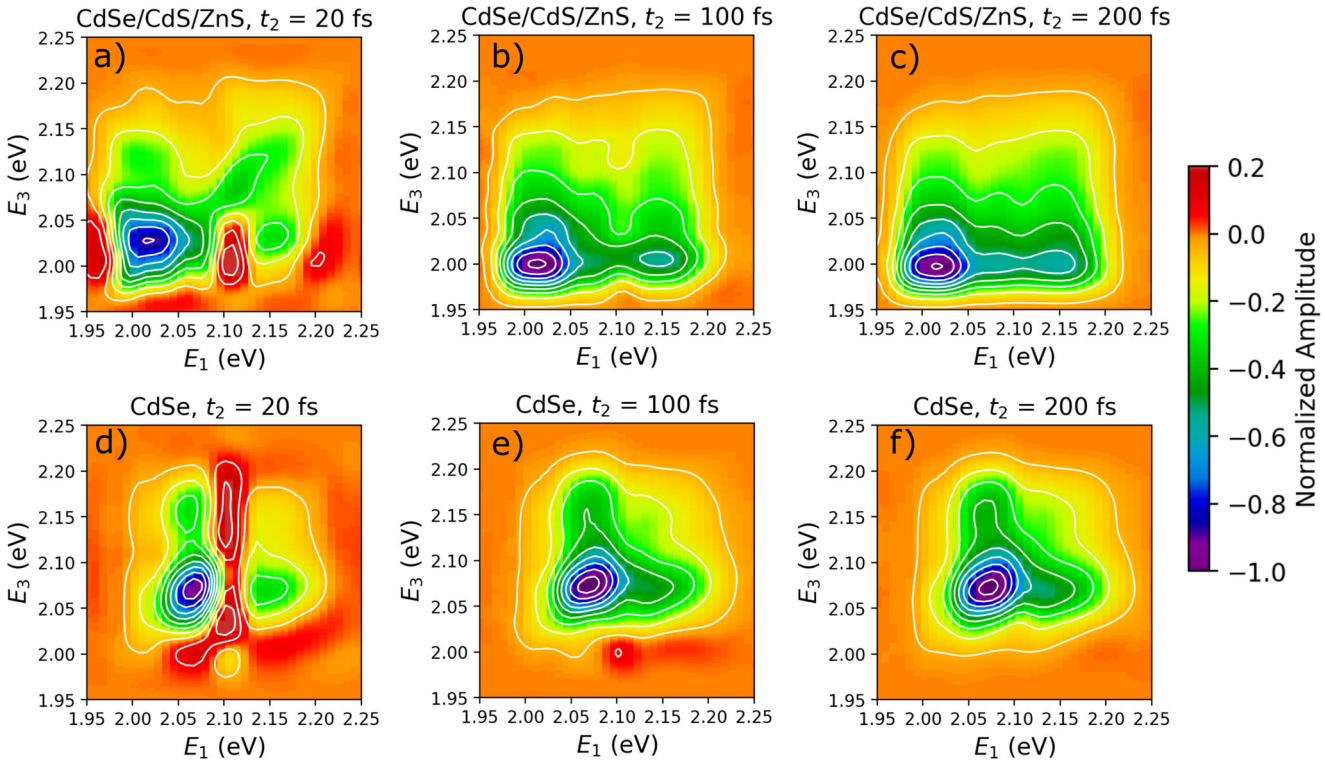

Fig. 2 Overview of two-dimensional electronic spectroscopy (2DES) signals as contour plots. Each panel corresponds to a fixed population time t_2, where t_2 is the time delay between the pump pulses and the probe pulse. **a**–**c** 2DES spectra of CdSe/CdS/ZnS at $t_2 = 20$ fs, 100 fs, and 200 fs. **d**–**f** 2DES spectra of CdSe at $t_2 = 20$ fs, 100 fs, and 200 fs. The color bar corresponds to the normalized amplitude of the 2DES signal. At $t_2 = 20$ fs the 2DE spectra are distorted due to the overlap between the three laser pulses. At $t_2 = 100$ fs the pulse overlap artifacts are gone. For CdSe/CdS/ZnS, the X_2–X_1 peak in lower right-hand corner grows between $t_2 = 100$ and 200 fs, while CdSe does not show significant change from $t_2 = 100$ to 200 fs.

terminate quickly in CdSe, the ESA signals redshifted relative to the bleach last up to 120 fs and show clear dependence on the excitation energy, as seen in Fig. 3c, d. These results are consistent with previous TA experiments, which have shown that probing the ESA feature while selectively exciting the X_1 or X_2 transitions reveals dynamics on timescales of several hundreds of femtoseconds, lasting much longer than the IRF-limited bleach dynamics[51,52].

Analyzing 2DE spectra in terms of X_1 or X_2 transitions is convenient for comparison with state-resolved pump-probe experiments, as in Fig. 3, but it over-simplifies the complexity of the excitonic manifold, which appears denser, as revealed by 2DE spectra. Figure 4 shows a more detailed view of the excitation frequency dependence of the ESA features in CdSe at early times. Figure 4a shows pseudo-TA spectra with X_1 and X_2 excitation, though the amplitude range is restricted to positive values and the probe range is restricted to the region of the ESA peak. Exciting the sample at X_1 results in ESA that decays in 80 fs, while exciting the sample at X_2 results in a buildup in the ESA signal on a 30 fs timescale followed by a decay lasting more than 100 fs. As will be discussed below, these data reveal a complex dynamical picture in which the dynamics involve manifolds of X_1 and X_2 excitonic states and transitions.

Orthogonal to pseudo-TA projections of the 2DES spectra are excitation axis projections where the probe energy, E_3, is kept constant (Fig. 4b). This projection allows one to monitor the excitation energy dependence of a process with the continuous resolution, rather than discretely exciting X_1 or X_2. Figure 4b shows an ESA excitation spectrum, where the probe energy, E_3, is kept at 1.99 eV. This plot interpolates between the three ESA lifetimes shown in Fig. 4a. If the excitonic structure in this region simply consisted of two states, X_1 and X_2, Fig. 4b would show two ESA lifetimes centered at 2.065 and 2.165 eV, respectively. Rather, the ESA lifetime gradually increases across the excitation spectrum, reflecting sequential relaxation through an underlying continuum of states with varying ESA lifetimes. These signals reflect complex and continuous quantum dynamics between states rather than mere, two-state kinetics.

Similarly, 1D TA experiments[41] and 2DES experiments[31,41] have revealed that the biexcitonic spectrum is a complex manifold of states and many ESA pathways are available, forming a spectrum that can shift over time. ESA can be a sensitive probe of the excitonic fine structure, as bright and dark single-exciton states can couple to different multi-exciton states[33,42]. Figure 4c shows how relaxation within a manifold of excitonic states can be reflected in the ESA dynamics. The excitation pulse initially populates a subset of the bright states. If the system is probed immediately, at $t_2 = 0$ fs, there would be strong ESA from those bright states into the manifold of biexciton states, XX. If the system is allowed to evolve and probed at $t_2 = 150$ fs, non-radiative relaxation would have occurred, and the initial ESA pathway would be weaker. Increasing the excitation energy would excite states higher in the manifold and elongate nonradiative relaxation times. Without this nonradiative relaxation step, the ESA intensity should remain constant after the initial excitation and remain independent of t_2. ESA decay with an X_1 pump confirms that a manifold of states within X_1 must be present. Figure 4d shows the ESA pathways with X_2 excitation at $t_2 = 0$ fs and $t_2 = 150$ fs. Under these excitation conditions, one would expect a sequential relaxation from the X_2 manifold to the X_1 manifold, occurring on a 30 fs timescale based off the bleach dynamics in Fig. 3d, and then further relaxation within the X_1 manifold, occurring on an 80 fs timescale. The GSB and ESA dynamics reflect the same nonradiative relaxation pathways from X_2 to X_1 and from bright to dim states, though the ESA can

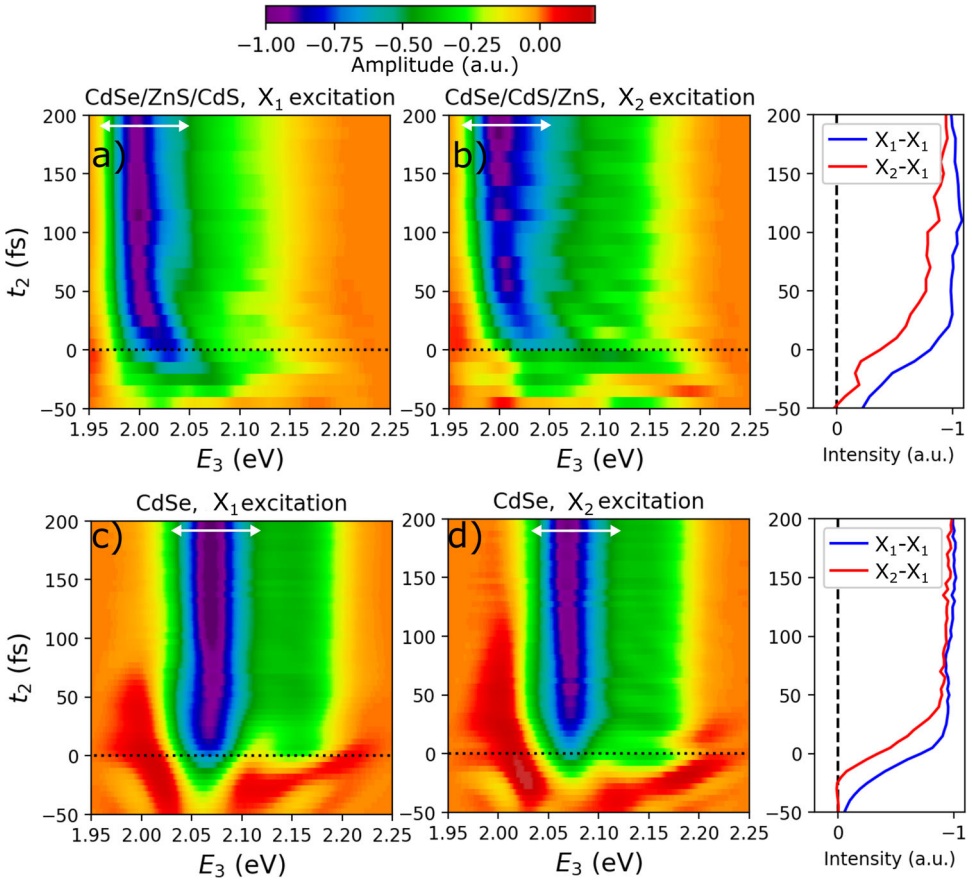

Fig. 3 Two-dimensional electronic spectroscopy (2DES) projections reveal exciton dynamics. Projecting the 2DES spectra along the E_3 axis to produce pseudotransient absorption (pseudo-TA) spectra. **a**, **b** Pseudo-TA spectra of CdSe/CdS/ZnS QD for X_1 and X_2 excitation, respectively. The side panel shows projections of the X_1–X_1 (blue) and X_2–X_1 (red) peaks for CdSe/CdS/ZnS. **c**, **d** Pseudo-TA spectra of CdSe QD for X_1 and X_2 excitation, respectively. The side panel shows projections of the X_1–X_1 (blue) and X_2–X_1(red) peaks for CdSe. White arrows in (**a**–**d**) show the integration area for generating the transients. The color bar corresponds to the normalized amplitude of the 2DES signal in (**a**–**d**).

provide additional information as the amplitude and energy of the ESA transition (X to XX) can shift with the relaxation within the single-exciton manifold. Moreover, the transition moments need not be the same absorbing from the ground state versus absorbing from the excited state, allowing the ESA to be a more sensitive probe of the nonradiative relaxation than the GSB.

Electronic structure calculations. To better understand the rapid relaxation dynamics of the X_1 and X_2 excitations and the significant differences between core and core/shell QDs, we first perform atomistic electronic structure calculations within the semiempirical pseudopotential approach combined with the Bethe–Salpeter equation[53–56] to delineate the excitonic states contributing to each transition. In the multiband effective mass approximation, the X_1 transition is comprised of a single electron–hole pair state, 1Sh-1Se, and similarly, the X_2 transition is comprised of the 2Sh–1Se electron–hole pair state[57]. As shown in Fig. 5b, c, the results based on the atomistic electronic structure calculations provide a different picture for CdSe and CdSe/CdS core–shell QDs[58]. We find that, for both systems, roughly 60 excitonic states contribute to the X_1 and X_2 transitions, though only a subset of the states has strong oscillator strengths, denoted as "bright" states. These bright states cluster together, forming the X_1 and X_2 transitions in the linear absorption spectrum. In addition to these bright states is a quasi-continuum of "dim" states that have weak oscillator strengths. The "bright" states can be initially excited by the excitation pulse while the "dim" states can be accessed through nonradiative relaxation from bright states. The term "dim" state is used here to generally denote exciton states with a weak oscillator strength as opposed to previously discussed "dark" states[59], which are spin-forbidden transitions. The relatively dense manifolds of excitonic states that comprise the X_1 and X_2 transitions have gaps that are smaller than the phonon frequencies in these systems, enabling single-phonon and efficient multi-phonon emission processes that lead to fast cooling for both the core and core/shell QDs[60–62].

Next, we address the differences in the observed bleaching dynamics between CdSe and CdSe/CdS/ZnS, which have been previously attributed to the shell preventing surface trapping of holes[15,23]. However, recent 1D TA experiments with 10 fs resolution show no evidence of ultrafast hole trapping in core-only CdSe[17] and our TA measurements with 50 fs time resolution reveal hole trapping on timescales of tens of picoseconds[34]. Given the absence of evidence of ultrafast hole trapping, the observed 30 fs dynamics of the optical bleach is attributed to hole relaxation. Fig. 5a shows the calculated phonon spectral densities, or the densities of phonon states weighted by the exciton–phonon coupling, for CdSe and CdSe/CdS QDs. The reorganization energy, λ, calculated as the phonon spectral density integrated over frequencies[63], is ~19 meV for CdSe while the reorganization energy is ~4 meV for CdSe/CdS. The calculations reveal a nearly complete attenuation of the low energy phonon modes in CdSe/CdS QDs but the intensity of the LO phonon peak is similar in both samples, consistent with the LO phonon coupling observed in the 2DES transients (Supplementary Fig. S15). These results are consistent with previous experiments, which show that the strength of the

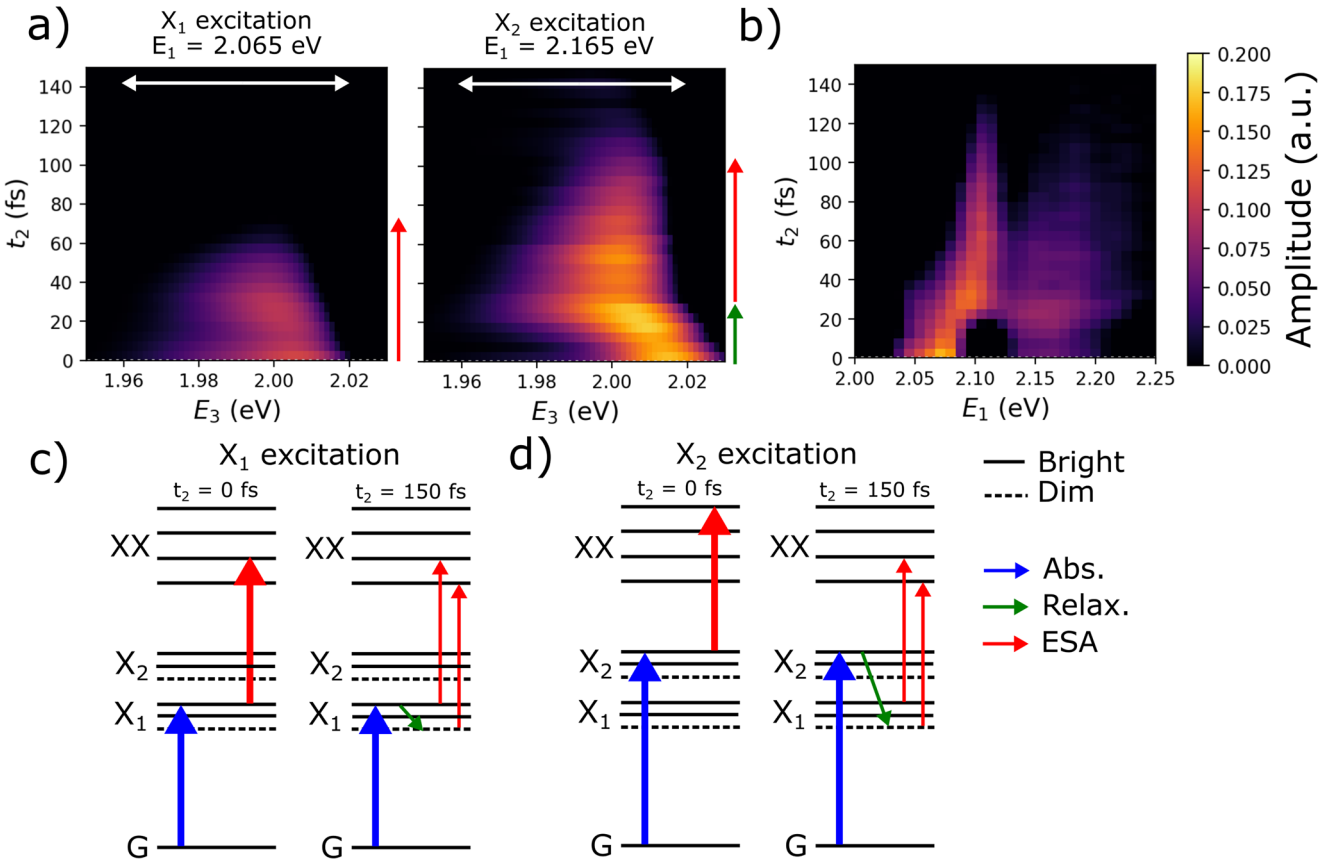

Fig. 4 Excited-state absorption (ESA) signals in CdSe quantum dots projected onto the emission and excitation axes. a Pseudo-TA spectra of CdSe QDs with X_1 and X_2 excitation. X_2 excitation results in an initial buildup followed by a decay. White arrows in panels a show the integration area for generating the plot in (**b**). **b** Projection of the ESA feature onto t_2 and the excitation energy E_1 shows that the ESA lifetime increases with excitation energy. The color bar corresponds to the amplitude of the ESA signal, truncating just the signal with positive amplitude. **c** Level diagrams show the intensity of the ESA transition reflects nonradiative relaxation within the manifold of X_1 states with X_1 excitation. **d** X_2 excitation results in successive relaxation from X_2 to X_1 and relaxation within the manifold of X_1 states.

exciton–phonon coupling decreases with the addition of a thin shell onto CdSe nanostructures[63–66]. This reduction in exciton–phonon coupling can be attributed to the localization of the hole to the CdSe core in quasi-type II core/shell structures like CdSe/CdS, which suppresses exciton–phonon coupling to delocalized phonon modes with frequencies less than 15 meV (Fig. 5a)[63]. As the observed X_2–X_1 relaxation process is phonon-mediated, the weaker exciton–phonon coupling in CdSe/CdS would result in a slower relaxation of the core–shell system, as observed experimentally.

To further understand the differences between core and core/shell QDs, we examine the relative contributions of single-particle hole and electron states to the correlated, two-particle excitonic states comprising the X_1 and X_2 transitions. Figure 5d shows that, in CdSe, every excitonic state in the range of the X_1 and X_2 transitions share the same dominant, band-edge electron state but differs in the hole state. Therefore, in CdSe, exciting the X_2 transition and probing the X_1 transition would resolve solely hole dynamics, consistent with earlier models[22,51]. In CdSe/CdS core–shell QDs the conduction bands of the CdSe and CdS layers are nearly degenerate and the electronic wavefunction is delocalized into the CdS layers while the hole remains localized in the CdSe core[67,68], as shown in the inset in Fig. 5e. This behavior qualitatively changes the nature of the excitonic states comprising the X_2 transition in CdSe/CdS, as shown in Fig. 5d. The current calculations confirm previous work showing that delocalization of the electron and hole wavefunctions into the CdS shell significantly alters the exciton energy levels[39,68,69]. There is still significant variation in the single-particle hole states, but the single-particle electron state also varies, signifying that higher-energy electronic states, not just the electronic state at the band edge, contribute to excitonic states in the X_2 transition. This result indicates that relaxation from X_2 to X_1 in core/shell QDs involves both electron and hole dynamics. The presence of hot electronic states could slow the exciton relaxation as electron–phonon coupling is much weaker than hole-phonon coupling[22,70]. Therefore, phonon-mediated exciton relaxation that involves both electrons and holes in CdSe/CdS/ZnS may be slower than the hole-dominated relaxation occurring in core-only CdSe, further explaining the differences in the observed timescales. These observations suggest that the core/shell system is significantly different from the core-only system, both in terms of excitonic structure and exciton–phonon coupling.

Conclusions. The contribution of holes to the bleaching signals in QDs is a decades-old controversy. We exploit the unique energy and time resolution of 2DE spectroscopy to reveal the missing hole signals in CdSe QDs after decades of searching via 1D spectroscopy. The 2DES experiments on core-only QDs reveal an ultrafast 30 fs timescale, which we attribute to hot hole relaxation, that is too fast to be observed by other experimental methods. The experiments reveal complex quantum dynamics between manifolds of states that do not follow simple kinetics. Atomistic calculations reveal qualitative differences between core-only and core/shell QDs in both excitonic structure and coupling to phonons, which explains the order of magnitude difference in the

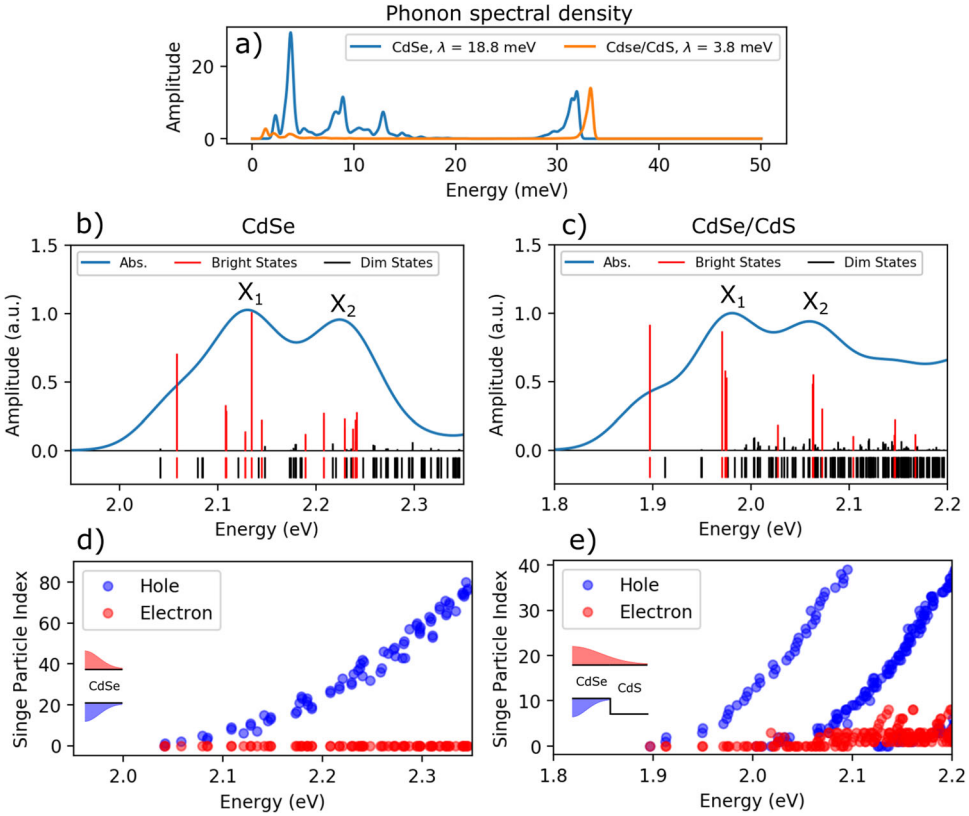

Fig. 5 Atomistic calculations of exciton and phonon states as well as exciton–phonon couplings in CdSe quantum dots (QDs) and CdSe/CdS QDs. **a** The calculated phonon spectral density for CdSe QDs (blue) and CdSe/CdS QDs (orange) shows stronger exciton–phonon coupling for CdSe QDs. Calculated linear absorption spectra of (**b**) CdSe QDs and **c** CdSe/CdS QDs, featuring "bright states" with stronger oscillator strength (red) and "dim states" that are weakly coupled to the ground state (black). **d** In CdSe QDs, projecting the two-particle excitonic wavefunctions onto single-particle states shows that higher-energy excitonic states differ in terms of their hole states (blue circles) but have the same band-edge electron state (red circles). **e** In CdSe/CdS QDs, projections onto single-particle states show that higher excitonic states consist of higher-energy electronic states.

observed dynamics. These experiments and calculations, in addition to revealing missing hole signals, reveal the importance of atomistic details in the behavior of real QD.

Methods

Pulse generation. The light pulses for 2DES are generated by a Ti:Sapphire amplifier (Coherent Legend Elite Duo HE + , 800 nm, 1 kHz, 130 fs) seeding a commercial optical parametric amplifier (TOPAS). The optical parametric amplifier output at 600 nm is broadened in a hollow core fiber filled with 3 atm of argon[71]. This spectrum is temporally stretched in a grism pair before being split between two acousto-optic pulse shapers (Fastlite, Dazzler). The pulse shapers apply a phase mask to the spectrum to compress the pulse and an amplitude mask to shape the spectrum into a super-Gaussian shape. The measured pulse length is 17 fs, as shown in Supplementary Note 6.

Two-dimensional electronics spectroscopy. The experimental setup is depicted in Fig. 1a. One of the pulse shapers diffracts two pulses, separated by a time delay t_1 and phase difference φ, to be used as a pump beam. The other pulse shaper diffracts a single pulse to act as the probe. The pump beam crosses the sample at an angle and is stopped by a beam block while the probe is transmitted straight through the sample and into a CCD spectrometer (Acton 2500i, PIXIS 100B Excelon). To measure a single 2DES spectrum, the time delay between the pump and probe pulses, t_2, is kept constant while the time delay between the two pump pulses, t_1, is varied. A $2 \times 2 \times 1$ phase cycling scheme is used where the phase of the first two pulses is set to $\varphi = 0$ and $\varphi = \pi$ for each value of t_1. Time delay t_1 is incremented in steps of 3 fs from 0 fs to 120 fs. A rotating frame with a frequency of 0.408 PHz is applied to the second pulse relative to the first pulse. The data is Fourier transformed along t_1 to generate a two-dimensional (E_1, E_3) map. A pulse energy of 5 nJ/pulse was used for each of the three pulses.

Materials. CdSe QD was purchased from NNlabs with a diameter of 4.6 nm. CdSe/CdS/ZnS core/shell QD were synthesized using previously published techniques[72,73].

Theoretical methods. Atomistic electronic structure calculations were performed within the semiempirical pseudopotential method[55]. The filter diagonalization technique was used to obtain single-particle electron and hole states near the band edge, which were then used as input to the Bethe–Salpeter equation to obtain correlated excitonic states. The phonon frequencies and modes of the nanocrystal are obtained via diagonalization of the dynamical matrix, computed with LAMMPS using the same Stillinger–Weber interaction potential. The exciton–phonon coupling matrix elements are then computed to first order in atomic displacements[70]. These couplings are used to compute the reorganization energy and spectral density, or weighted density of phonon states. All calculations were performed on fully passivated QD structures relaxed using molecular dynamics-based geometry optimization[74,75]. Additional details are included in the Supplementary Methods.

Data availability

Data are available from the corresponding author upon reasonable request.

Code availability

Computer code is available from the corresponding author upon reasonable request.

Received: 4 July 2022; Accepted: 27 February 2023;
Published online: 16 March 2023

References

1. Talapin, D. V., Lee, J. S., Kovalenko, M. V. & Shevchenko, E. V. Prospects of colloidal nanocrystals for electronic and optoelectronic applications. *Chem. Rev.* **110**, 389–458 (2010).
2. Scholes, G. D. & Rumbles, G. Excitons in nanoscale systems. *Nat. Mater.* **5**, 683–696 (2006).

3. Pietryga, J. M. et al. Spectroscopic and device aspects of nanocrystal quantum dots. *Chem. Rev.* **116**, 10513–10622 (2016).
4. Efros, A. L. & Brus, L. E. Nanocrystal quantum dots: from discovery to modern development. *ACS Nano* **15**, 6192–6210 (2021).
5. Kovalenko, M. V. et al. Prospects of nanoscience with nanocrystals. *ACS Nano* **9**, 1012–1057 (2015).
6. Liu, M. et al. Colloidal quantum dot electronics. *Nat. Electron.* **4**, 548–558 (2021).
7. Chen, Y. et al. Giant" multishell CdSe nanocrystal quantum dots with suppressed blinking. *J. Am. Chem. Soc.* **130**, 5026–5027 (2008).
8. Fisher, B., Caruge, J. M., Zehnder, D. & Bawendi, M. Room-temperature ordered photon emission from multiexciton states in single CdSe core-shell nanocrystals. *Phys. Rev. Lett.* **94**, 1–4 (2005).
9. Fisher, B. R., Eisler, H. J., Stott, N. E. & Bawendi, M. G. Emission intensity dependence and single-exponential behavior in single colloidal quantum dot fluorescence lifetimes. *J. Phys. Chem. B* **108**, 143–148 (2004).
10. Klimov, V. I. Optical nonlinearities and ultrafast carrier dynamics in semiconductor nanocrystals. *J. Phys. Chem. B* **104**, 6112–6123 (2000).
11. Klimov, V. I. et al. Optical gain and stimulated emission in nanocrystal quantum dots. *Science* **290**, 314–317 (2000).
12. Guyot-Sionnest, P. & Hines, M. A. Intraband transitions in semiconductor nanocrystals. *Appl. Phys. Lett.* **72**, 686–688 (1998).
13. Klimov, V. I. Spectral and dynamical properties of multiexcitons in semiconductor nanocrystals. *Annu. Rev. Phys. Chem.* **58**, 635–673 (2007).
14. Abdellah, M. et al. Hole trapping: the critical factor for quantum dot sensitized solar cell performance. *J. Phys. Chem. C.* **118**, 25802–25808 (2014).
15. Grimaldi, G. et al. Spectroscopic evidence for the contribution of holes to the bleach of Cd-chalcogenide quantum dots. *Nano Lett.* **19**, 3002–3010 (2019).
16. Morgan, D. P. & Kelley, D. F. What does the transient absorption spectrum of CdSe quantum dots measure? *J. Phys. Chem. C.* **124**, 8448–8455 (2020).
17. Dana, J. et al. Testing the fate of nascent holes in CdSe nanocrystals with sub-10 fs pump-probe spectroscopy. *Nanoscale* **13**, 1982–1987 (2021).
18. He, S., Li, Q., Jin, T. & Lian, T. Contributions of exciton fine structure and hole trapping on the hole state filling effect in the transient absorption spectra of CdSe quantum dots. *J. Chem. Phys.* **156**, 054704 (2022).
19. Yuan, J. et al. Metal halide perovskites in quantum dot solar cells: progress and prospects. *Joule* **4**, 1160–1185 (2020).
20. Park, Y. S., Roh, J., Diroll, B. T., Schaller, R. D. & Klimov, V. I. Colloidal quantum dot lasers. *Nat. Rev. Mater.* **6**, 382–401 (2021).
21. Moon, H., Lee, C., Lee, W., Kim, J. & Chae, H. Stability of quantum dots, quantum dot films, and quantum dot light-emitting diodes for display applications. *Adv. Mater.* **31**, 1804294 (2019).
22. Sewall, S. L., Cooney, R. R. & Kambhampati, P. Experimental tests of effective mass and atomistic approaches to quantum dot electronic structure: ordering of electronic states. *Appl. Phys. Lett.* **94**, 205–207 (2009).
23. Taheri, M. M. et al. Distinguishing electron and hole dynamics in functionalized CdSe/CdS core/shell quantum dots using complementary ultrafast spectroscopies and kinetic modeling. *J. Phys. Chem. C.* **125**, 31–41 (2021).
24. Sewall, S. L. et al. State-resolved studies of biexcitons and surface trapping dynamics in semiconductor quantum dots. *J. Chem. Phys.* **129**, 084701 (2008).
25. Tyagi, P. & Kambhampati, P. False multiple exciton recombination and multiple exciton generation signals in semiconductor quantum dots arise from surface charge trapping. *J. Chem. Phys.* **134**, 094706 (2011).
26. Fuller, F. D. & Ogilvie, J. P. Experimental implementations of two-dimensional fourier transform electronic spectroscopy. *Annu. Rev. Phys. Chem.* **66**, 667–690 (2015).
27. Jarrett, J. W. et al. Dissecting charge relaxation pathways in CdSe/CdS nanocrystals using femtosecond two-dimensional electronic spectroscopy. *Nanoscale* **9**, 4572–4577 (2017).
28. Stoll, T. et al. Two-Dimensional electronic spectroscopy unravels sub-100 fs electron and hole relaxation dynamics in Cd-chalcogenide nanostructures. *J. Phys. Chem. Lett.* **8**, 2285–2290 (2017).
29. Lenngren, N. et al. Hot electron and hole dynamics in thiol-capped CdSe quantum dots revealed by 2D electronic spectroscopy. *Phys. Chem. Chem. Phys.* **18**, 26199–26204 (2016).
30. Griffin, G. B. et al. Two-dimensional electronic spectroscopy of CdSe nanoparticles at very low pulse power. *J. Chem. Phys.* **138**, 014705 (2013).
31. Seiler, H., Palato, S., Sonnichsen, C., Baker, H. & Kambhampati, P. "Seeing multiexcitons through sample inhomogeneity: band-edge biexciton structure in CdSe nanocrystals revealed by two-dimensional electronic spectroscopy. *Nano Lett.* **18**, 2999–3006 (2018).
32. Wong, C. Y. & Scholes, G. D. Biexcitonic fine structure of CdSe nanocrystals probed by polarization-dependent two-dimensional photon echo. *Spectroscopy* **115**, 3797–3806 (2011).
33. Sewall, S. L., Franceschetti, A., Cooney, R. R., Zunger, A. & Kambhampati, P. Direct observation of the structure of band-edge biexcitons in colloidal semiconductor CdSe quantum dots. *Phys. Rev. B Condens. Matter Mater. Phys.* **80**, 1–4 (2009).
34. Sewall, S. L., Cooney, R. R., Dias, E. A., Tyagi, P. & Kambhampati, P. State-resolved observation in real time of the structural dynamics of multiexcitons in semiconductor nanocrystals. *Phys. Rev. B Condens. Matter Mater. Phys.* **84**, 1–8 (2011).
35. Park, S. D. et al. Bandgap inhomogeneity of a PbSe quantum dot ensemble from two-dimensional spectroscopy and comparison to size inhomogeneity from electron microscopy. *Nano Lett.* **17**, 762–771 (2017).
36. Liu, A., Almeida, D. B., Bae, W. K., Padilha, L. A. & Cundiff, S. T. Non-Markovian exciton-phonon interactions in core-shell colloidal quantum dots at femtosecond timescales. *Phys. Rev. Lett.* **123**, 57403 (2019).
37. Wong, C. Y. & Scholes, G. D. Using two-dimensional photon echo spectroscopy to probe the fine structure of the ground state biexciton of CdSe nanocrystals. *J. Lumin.* **131**, 366–374 (2011).
38. Deka, S. et al. CdSe/CdS/ZnS double shell nanorods with high photoluminescence efficiency and their exploitation as biolabeling probes. *J. Am. Chem. Soc.* **131**, 2948–2958 (2009).
39. Bisschop, S., Geiregat, P., Aubert, T. & Hens, Z. The impact of core/shell sizes on the optical gain characteristics of CdSe/CdS quantum dots. *ACS Nano* **12**, 9011–9021 (2018).
40. Vonk, S. J. W. et al. Biexciton binding energy and line width of single quantum dots at room temperature. *Nano Lett.* **21**, 5760–5766 (2021).
41. Palato, S. et al. Investigating the electronic structure of confined multiexcitons with nonlinear spectroscopies. *J. Chem. Phys.* **152**, 104710 (2020).
42. Korkusinski, M., Voznyy, O. & Hawrylak, P. Fine structure and size dependence of exciton and biexciton optical spectra in CdSe nanocrystals. *Phys. Rev. B Condens. Matter Mater. Phys.* **82**, 1–16 (2010).
43. Rodina, A. V. & Efros, A. L. Band-edge biexciton in nanocrystals of semiconductors with a degenerate valence band. *Phys. Rev. B Condens. Matter Mater. Phys.* **82**, 1–14 (2010).
44. Califano, M., Franceschetti, A. & Zunger, A. Lifetime and polarization of the radiative decay of excitons, biexcitons, and trions in CdSe nanocrystal quantum dots. *Phys. Rev. B Condens. Matter Mater. Phys.* **75**, 1–7 (2007).
45. Rodek, A. et al. Local field effects in ultrafast light-matter interaction measured by pump-probe spectroscopy of monolayer $MoSe_2$. *Nanophotonics* **10**, 2717–2728 (2021).
46. Mondal, R., Roy, B., Pal, B. & Bansal, B. How pump-probe differential reflectivity at negative delay yields the perturbed-free-induction-decay: theory of the experiment and its verification. *J. Phys. Condens. Matter* **30**, 505902 (2018).
47. Wolpert, C. et al. Ultrafast coherent spectroscopy of a single self-assembled quantum dot. *Phys. Status Solidi Basic Res.* **249**, 721–730 (2012).
48. Yan, S., Seidel, M. T. & Tan, H. S. Perturbed free induction decay in ultrafast mid-IR pump-probe spectroscopy. *Chem. Phys. Lett.* **517**, 36–40 (2011).
49. Nuernberger, P. et al. Noise in experimental ultrafast pump–probe data. *Opt. Lett.* **34**, 3226–3228 (2009).
50. Paleček, D., Edlund, P., Gustavsson, E., Westenhoff, S. & Zigmantas, D. Potential pitfalls of the early-time dynamics in two-dimensional electronic spectroscopy. *J. Chem. Phys.* **151**, 024201 (2019).
51. Cooney, R. R., Sewall, S. L., Anderson, K. E. H., Dias, E. A. & Kambhampati, P. Breaking the phonon bottleneck for holes in semiconductor quantum dots. *Phys. Rev. Lett.* **98**, 1–4 (2007).
52. Schnitzenbaumer, K. J., Labrador, T. & Dukovic, G. Impact of chalcogenide ligands on excited state dynamics in CdSe quantum dots. *J. Phys. Chem. C.* **119**, 13314–13324 (2015).
53. Wang, L. W. & Zunger, A. Electronic structure pseudopotential calculations of large (approximately 1000 atoms) Si quantum dots. *J. Phys. Chem.* **98**, 2158–2165 (1994).
54. Wang, L. W. & Zunger, A. Pseudopotential calculations of nanoscale CdSe quantum dots. *Phys. Rev. B Condens. Matter Mater. Phys.* **53**, 9579–9582 (1996).
55. Rabani, E., Hetényi, B., Berne, B. J. & Brus, L. E. Electronic properties of CdSe nanocrystals in the absence and presence of a dielectric medium. *J. Chem. Phys.* **110**, 5355–5369 (1999).
56. Jasrasaria, D., Weinberg, D., Philbin, J. P. & Rabani, E. Simulations of nonradiative processes in semiconductor nanocrystals. *J. Chem. Phys.* **157**, 020901 (2022).
57. Efros, A. L. & Rosen, M. Electronic structure of semiconductor nanocrystals. *Annu. Rev. Mater. Sci.* **30**, 475–521 (2000).
58. Wang, L. W. & Zunger, A. High-energy excitonic transitions in CdSe quantum dots. *J. Phys. Chem. B* **102**, 6449–6454 (1998).
59. Nirmal, M. et al. Observation of the "dark exciton" in CdSe quantum dots. *Phys. Rev. Lett.* **75**, 3728–3731 (1995).
60. Kambhampati, P. Hot exciton relaxation dynamics in semiconductor quantum dots: radiationless transitions on the nanoscale. *J. Phys. Chem.* **115**, 22089–22109 (2011).
61. Kilina, S. V., Kilin, D. S. & Prezhdo, O. V. Breaking the phonon bottleneck in PbSe and CdSe quantum dots: time-domain density functional theory of charge carrier relaxation. *ACS Nano* **3**, 93–99 (2009).

62. Sagar, D. M. et al. Size dependent, state-resolved studies of exciton-phonon couplings in strongly confined semiconductor quantum dots. *Phys. Rev. B Condens. Matter Mater. Phys.* **77**, 1–14 (2008).
63. Lin, C., Gong, K., Kelley, D. F. & Myers Kelley, A. Electron-phonon coupling in CdSe/CdS core/shell quantum dots. *ACS Nano* **9**, 8131–8141 (2015).
64. Dzhagan, V. M. et al. The influence of shell parameters on phonons in core–shell nanoparticles: a resonant Raman study. *Nanotechnology* **20**, 1–6 (2009).
65. Achtstein, A. W. et al. Impact of shell growth on recombination. *ACS Nano* **12**, 9476–9483 (2018).
66. Scott, R. et al. A comparative study demonstrates strong size tunability of carrier–phonon coupling in CdSe-based 2D and 0D nanocrystals. *Nanoscale* **11**, 3958–3967 (2019).
67. Balan, A. D. et al. Effect of thermal fluctuations on the radiative rate in core/shell quantum dots. *Nano Lett.* **17**, 1629–1636 (2017).
68. Nandan, Y. & Mehata, M. S. Wavefunction engineering of type-I/type-II excitons of CdSe/CdS core-shell quantum dots. *Sci. Rep.* **9**, 1–11 (2019).
69. Mehata, M. S. & Ratnesh, R. K. Luminescence properties and exciton dynamics of core-multi-shell semiconductor quantum dots leading to QLEDs. *Dalton Trans.* **48**, 7619–7631 (2019).
70. Jasrasaria, D. & Rabani, E. Interplay of surface and interior modes in exciton-phonon coupling at the nanoscale. *Nano Lett.* **21**, 8741–8748 (2021).
71. Sonnichsen, C., Brosseau, P., Reid, C. & Kambhampati, P. OPA-driven hollow-core fiber as a tunable, broadband source for coherent multidimensional spectroscopy. *Opt. Express* **29**, 28352 (2021).
72. Boldt, K., Kirkwood, N., Beane, G. A. & Mulvaney, P. Synthesis of highly luminescent and photo-stable, graded shell CdSe/Cd xZn1-xS nanoparticles by in situ alloying. *Chem. Mater.* **25**, 4731–4738 (2013).
73. Chen, O. et al. Compact high-quality CdSe-CdS core-shell nanocrystals with narrow emission linewidths and suppressed blinking. *Nat. Mater.* **12**, 445–451 (2013).
74. Zhou, X. W. et al. Stillinger-Weber potential for the II-VI elements Zn-Cd-Hg-S-Se-Te. *Phys. Rev. B Condens. Matter Mater. Phys.* **88**, 1–14 (2013).
75. Plimpton, S. Fast parallel algorithms for short-range molecular dynamics. *J. Comput. Phys.* **117**, 1–19 (1995).

Acknowledgements

E.R. acknowledges support from the Department of Energy, Photonics at the Thermodynamic Limits Energy Frontier Research Center, under grant no. DESC0019140. Methods used in this work were provided by the Center for Computational Study of Excited State Phenomena in Energy Materials (C2SEPEM), which is funded by the U.S. Department of Energy, Office of Science, Basic Energy Sciences, Materials Sciences and Engineering Division, via contract no. DE-AC02- 05CH11231, as part of the Computational Materials Sciences Program. Computational resources were provided by the National Energy Research Scientific Computing Center (NERSC), a U.S. Department of Energy Office of Science User Facility operated under contract no. DE-AC02-05CH11231. D.J. acknowledges the support of the Computational Science Graduate Fellowship from the U.S. Department of Energy under grant no. DE-SC0019323. A.J.H. and J.J.G. acknowledge financial support from the European Research Council Horizon 2020 ERC Grant Agreement No. 678004 (Doping on Demand). P.B. and P.K. acknowledge support from McGill University, NSERC, CFI, FQRNT, and Sony.

Author contributions

P.B. wrote the manuscript with revisions from P.K., J.G., A.H., D.J., and E.R. P.B. conducted the two-dimensional electronic spectroscopy experiments and conducted data analysis with input from P.K., J.G., and A.H. J.G. synthesized the CdSe/CdS/ZnS quantum dots. D.J. conducted the electronic structure calculations with supervision from E.R. All authors discussed the results and implications at all stages.

Competing interests

The authors declare no competing interests.

Additional information

Supplementary information The online version contains supplementary material available at https://doi.org/10.1038/s42005-023-01169-1.

Correspondence and requests for materials should be addressed to Patanjali Kambhampati.

Peer review information *Communications Physics* thanks Mohan Singh Mehata and the other, anonymous, reviewer(s) for their contribution to the peer review of this work.

Reprints and permission information is available at http://www.nature.com/reprints

Publisher's note Springer Nature remains neutral with regard to jurisdictional claims in published maps and institutional affiliations.